Report

Cell Reports

A Switch in Tissue Stem Cell Identity Causes Neuroendocrine Tumors in *Drosophila* Gut

Graphical Abstract

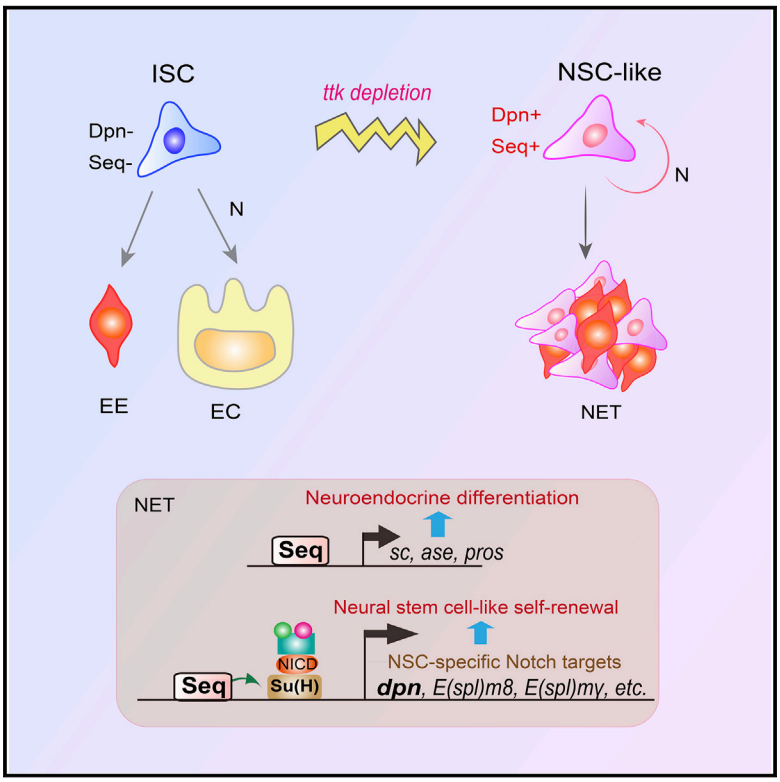

Highlights

- Depletion of ttk69 in fly ISCs causes a genome-wide program switch to NSC-like
- The ectopically expressed NSC factor Dpn drives NET tumorigenesis
- The ectopically expressed pan-neural factor Seq generates a neuroendocrine phenotype
- Seq also converts the differentiation-promoting role of Notch into a self-renewal role

Authors

Zhaohui Li, Xingting Guo, Huanwei Huang, ..., Zhen Jin, Tao Cai, Rongwen Xi

Correspondence

xirongwen@nibs.ac.cn

In Brief

Li et al. show that the loss of a transcriptional repressor, Tramtrack, in adult *Drosophila* intestinal stem cells causes a self-renewal program switch to neural-stem-cell-like, which drives neuroendocrine tumor development.

Li et al., 2020, Cell Reports *30*, 1724–1734
February 11, 2020
https://doi.org/10.1016/j.celrep.2020.01.041

CellPress

OPEN ACCESS
CellPress

Cell Reports
Report

A Switch in Tissue Stem Cell Identity Causes Neuroendocrine Tumors in *Drosophila* Gut

Zhaohui Li,[1,2,4] Xingting Guo,[1,4] Huanwei Huang,[1,4] Chenhui Wang,[1] Fu Yang,[1] Yongchao Zhang,[1] Jiawen Wang,[1] Lu Han,[1] Zhen Jin,[1] Tao Cai,[1] and Rongwen Xi[1,3,5,*]

[1]National Institute of Biological Sciences, No. 7 Science Park Road, Zhongguancun Life Science Park, Beijing 102206, China
[2]School of Life Sciences, Tsinghua University, Beijing 100084, China
[3]Tsinghua Institute of Multidisciplinary Biomedical Research, Tsinghua University, Beijing 102206, China
[4]These authors contributed equally
[5]Lead Contact
*Correspondence: xirongwen@nibs.ac.cn
https://doi.org/10.1016/j.celrep.2020.01.041

SUMMARY

Intestinal stem cells (ISCs) are able to generate gut-specific enterocytes, as well as neural-like enteroendocrine cells. It is unclear how the tissue identity of the ISC lineage is regulated to confer cell-lineage fidelity. Here, we show that, in adult *Drosophila* midgut, loss of the transcriptional repressor Tramtrack in ISCs causes a self-renewal program switch to neural stem cell (NSC)-like, and that switch drives neuroendocrine tumor development. In Tramtrack-depleted ISCs, the ectopically expressed Deadpan acts as a major self-renewal factor for cell propagation, and Sequoia acts as a differentiation factor for the neuroendocrine phenotype. In addition, the expression of Sequoia renders NSC-specific self-renewal genes responsive to Notch in ISCs, thus inverting the differentiation-promoting function of Notch into a self-renewal role as in normal NSCs. These results suggest an active maintenance mechanism for the gut identity of ISCs, whose disruption may lead to an improper acquisition of NSC-like traits and tumorigenesis.

INTRODUCTION

In addition to the nervous system, neuroendocrine (NE) cells are found in many non-neural tissues and can develop neoplasias that are known as NE tumors (NETs) (Oronsky et al., 2017). The NE cells in non-neural tissues display characteristics that are typical of neurons, such as membrane excitability and hormone secretion, yet many of these NEs are generated from adult stem cells of endodermal origin. It is, thus, intriguing how the tissue identity of stem cells is regulated and controlled to safeguard cell-lineage fidelity.

The intestinal epithelium in adult *Drosophila* midgut is maintained by intestinal stem cells (ISCs)—the multipotent cells that are capable of generating both absorptive enterocytes (ECs) and secretary enteroendocrine cells (EEs) (Micchelli and Perrimon, 2006; Ohlstein and Spradling, 2006; Figure 1A). EEs are neural-like cells and are able to secrete sets of hormone peptides that are similar to those secreted by NE cells in the *Drosophila* brain (Guo et al., 2019b; Nässel and Winther, 2010). While the initiation of EC generation is driven by Delta (Dl)/Notch-mediated lateral inhibition between the two immediate stem cell daughters (de Navascués et al., 2012; Ohlstein and Spradling, 2007), the initiation of EE generation occurs at the stem cell level (Biteau and Jasper, 2014; Chen et al., 2018; Zeng and Hou, 2015), with a transient expression of the proneural gene *Scute* (*Sc*) that induces ISCs to self-renew and to generate an EE progenitor cell (EEP). Each EEP then divides one more time before terminal differentiation to yield a pair of EEs (Chen et al., 2018; Guo et al., 2019b). *Sc* encodes a basic helix-loop-helix (bHLH) transcription factor and belongs to the *achaete-scute* gene complex (AS-C), a *Drosophila* proneural gene cluster that is expressed in neural progenitor cells and is important for the development of the embryonic central nervous system and sensory organs of both larva and adult (Campuzano and Modolell, 1992; Ghysen et al., 1993). Thus, it appears that there is a transient activation of neural-like programs in ISCs that directs EE generation from ISCs.

Tramtrack (*Ttk*, or *Ttk69 isoform*), which encodes a BTB-domain-containing transcriptional repressor, acts as a master repressor of the differentiation of EEs from ISCs (Wang et al., 2015). Depletion of *ttk* in ISCs causes de-repression of AS-C genes including *Sc* and *Asense* (*Ase*). The continuous expression of Sc and Ase directs ISCs to continuously generate EEs, leading to the formation of EE-like tumors, or NETs (Wang et al., 2015). One intriguing observation from the *ttk*-depleted ISCs is that continuous derepression of the differentiation-promoting factors does not compromise ISC maintenance, but continuous overexpression of Sc in normal ISCs will cause regional ISC loss over time (Chen et al., 2018). Here, we characterized the *ttk*-depleted ISCs and, surprisingly, found that the original self-renewal program of ISCs had switched to a neuroblast-like self-renewal program that is responsible for NET tumorigenesis.

RESULTS

ttk-Depleted ISCs Switch Their Self-Renewal Program into Neuroblast-like

Beyond the excessive EE phenotype characterized by an excessive number of Prospero (Pros)-positive cells, we found that the

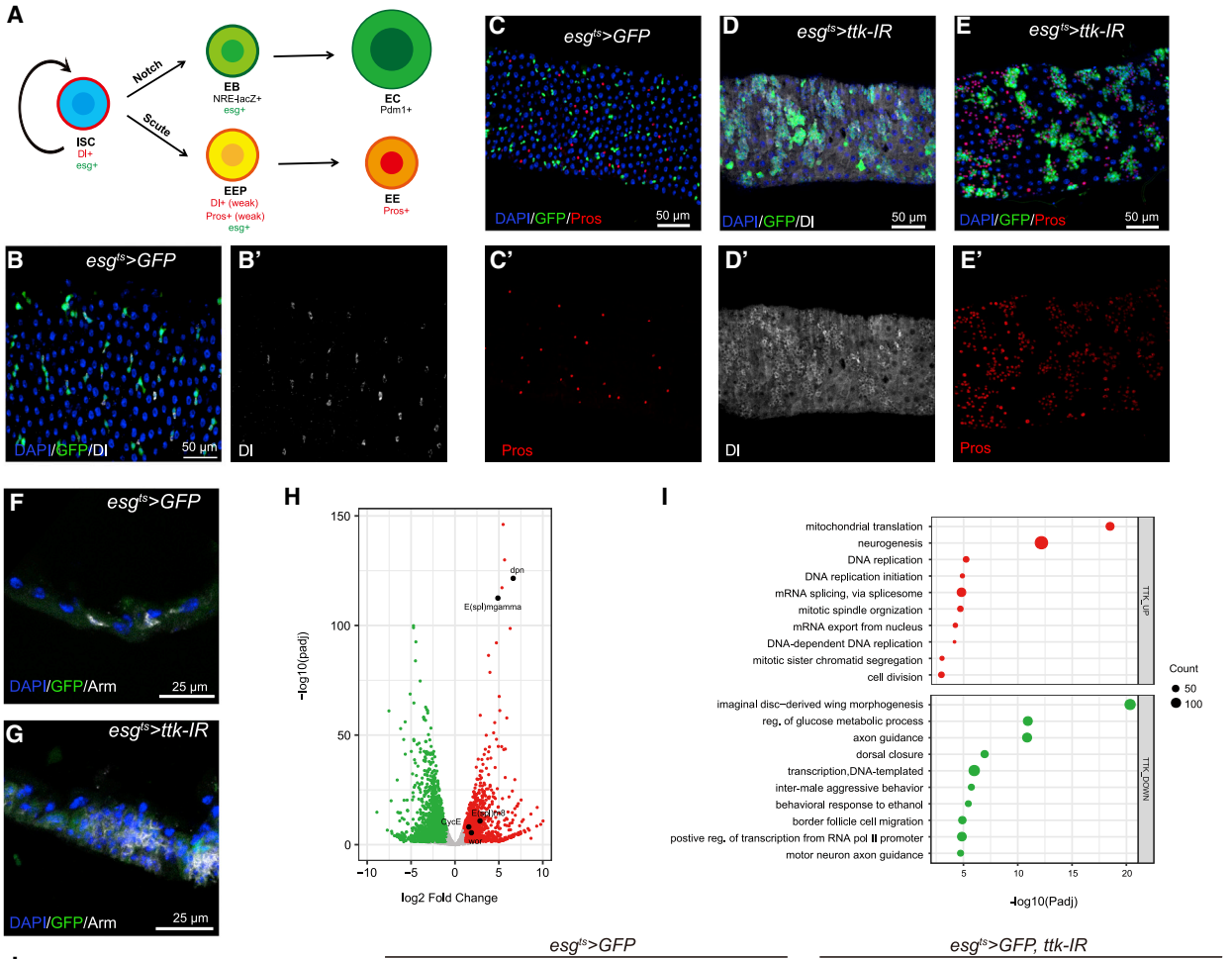

J

Gene	Log2(FC)	Padj
NB-specific genes		
dpn	6.58	8.70E-162
wor	1.83	8.90E-07
E(spl)mgamma-HLH	4.85	1.45E-115
E(spl)m8-HLH	2.81	3.62E-15
ase	3.86	3.14E-20
sna	1.58	1.63E-05
ISC-progenitor-specific genes		
esg	-1.09	3.94E-05
E(spl)mbeta-HLH	-3.49	7.01E-34
Df31	-1.6	2.54E-14
Myc	-3.01	8.19E-27
bun	-3.23	1.19E-52
E(spl)m3-HLH	-4.61	1.47E-56
N	-1.37	1.70E-10
peb	-2.51	2.17E-22
Blimp-1	-1.48	3.36E-08
fkh	-3.12	2.06E-64
mamo	-2.87	8.83E-44
Sox100B	-2.09	3.18E-17
Sox21a	-1.13	1.61E-05
klu	-1.48	7.85E-13
cic	-3.23	1.28E-60
fru	-2.25	8.80E-30
Rel	-1.23	1.07E-08

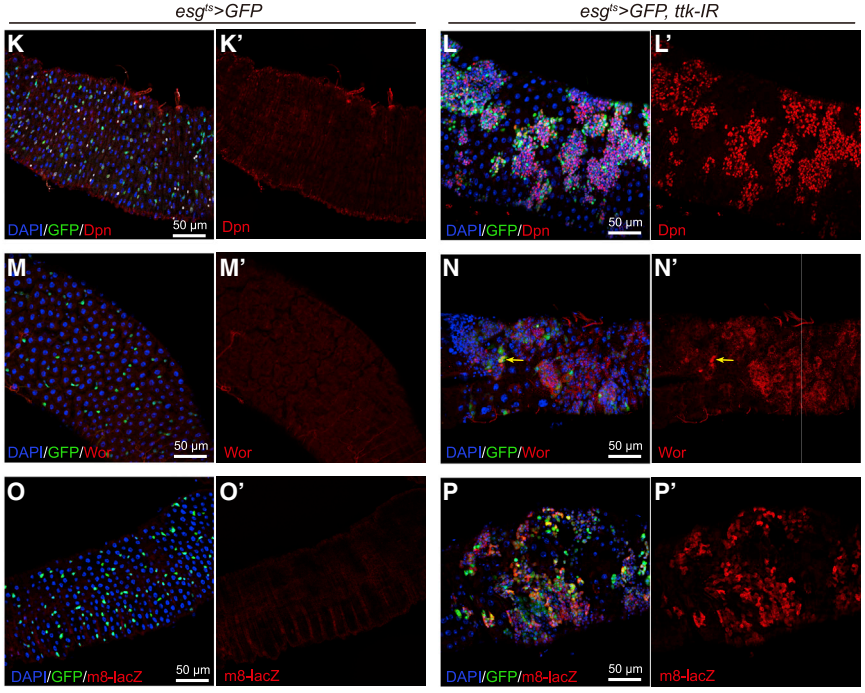

(legend on next page)

depletion of *ttk* in ISCs by RNAi targeting *ttk* (*esg^{ts}-Gal4, UAS-ttk-RNAi*, or *esg^{ts} > ttk-IR* for short) also caused generation of more esg$^+$ (marked by GFP) progenitor cells over time; these cells gradually cluster together and become multilayered tissues (Figures 1B–1G). This progenitor cell accumulation phenotype is not observed in ISCs with continuous Sc overexpression, and the latter one, instead, causes regional ISC loss, as continuous Sc expression will eventually compromise ISC maintenance by inducing their differentiation into EEs (Chen et al., 2018).

To investigate the mechanisms underlying this seemingly enhanced self-renewal ability of the tumor cells, we used fluorescence-activated cell sorting (FACS) to sort these esg > GFP$^+$ cells and performed gene expression analysis by RNA sequencing (RNA-seq). Compared to wild-type esg > GFP$^+$ cells, the *ttk*-depleted esg > GFP$^+$ cells showed significant upregulation of 1,887 genes and significant downregulation of 1,980 genes (Figure 1H). Gene Ontology (GO) analysis revealed that the majority of the top 10 upregulated gene categories include genes related to mitosis, DNA replication, and mitochondrial translation, which is consistent with the increased cell proliferation of *ttk*-depleted esg$^+$ cells. Notably, genes related to neurogenesis stand out as the only top upregulated gene category not related to cell proliferation (Figure 1I).

Interestingly, further examination of the upregulated neurogenesis genes revealed several neural-progenitor-specific transcription factor genes, including *worniu* (*wor*), as well as many *Enhancer-of-Split* (*Hes*) family genes, including *deadpan* (*dpn*), *E(spl)m8*, and *E(spl)mγ*, among others (Figure 1J). Notably, the transcription factors encoded by *dpn*, *wor*, and *E(spl)mγ* are known to serve as core components of the transcription factor network required for the self-renewal of *Drosophila* neuroblasts (NBs) (Berger et al., 2012; Zacharioudaki et al., 2012). Confirming the observations from our RNA-seq analysis, whole-mount *in situ* immunostaining with antibodies against Dpn and Wor revealed strong signals for these ectopically expressed proteins in *ttk*-depleted esg > GFP$^+$ cells, while no such signals were detected in normal midgut epithelial cells (Figures 1K–1N). Moreover, we also used a transcriptional reporter for *E(spl)m8* (*E(spl)m8-lacZ*) to successfully confirm the upregulation of *E(spl)m8* in *ttk*-depleted esg > GFP$^+$ cells (Figures 1O and 1P).

The top downregulated gene categories include wing morphogenesis, axon guidance, and glucose metabolism, and the latter one indicates the downregulation of digestion-related genes (Figure 1I); interestingly, 18 of the top 20 intestinal-progenitor-specific transcription factors (Doupé et al., 2018; Hung et al., 2018) showed significant downregulation following *ttk* depletion (Figure 1J), among which *esg* and *fkh* are known to be essential for ISC self-renewal, and *Sox100B* and *Sox21a* are known to be essential for ISC proliferation and differentiation (Chen et al., 2016; Doupé et al., 2018; Korzelius et al., 2014; Lan et al., 2018; Loza-Coll et al., 2014; Meng and Biteau, 2015; Zhai et al., 2015, 2017). These observations indicate that these formerly gut-like stem cells have undergone a genome-wide transcriptional switch and have acquired NB-like cell characteristics.

The Ectopic Dpn Expression Is Responsible for the Self-Renewal of *ttk*-Depleted Tumor Cells

The ectopic expression of neural stem cell (NSC) factors and the concomitant downregulation of expression of intestinal progenitor factors indicate that *ttk*-depleted mutant stem cells could have switched their stem cell identity and acquired a NB-like self-renewal program that drives improper cell proliferation and differentiation, thereby leading to NET formation. To test this hypothesis, we individually knocked down the observed upregulated NB-specific transcription factors and examined the attendant effects on *ttk*-depletion-induced NET formation. Interestingly, while individually depleting other NB-specific genes, including *E(spl)m8*, *E(spl)mγ* and *wor* did not yield any obvious phenotypic changes (data not shown), and the depletion of *dpn*, a known self-renewal factor for NBs (San-Juán and Baonza, 2011; Zacharioudaki et al., 2012), completely suppressed NET formation. In addition, the original esg$^+$ progenitor cells appeared to get lost from the gut over time (Figures 2A–2D). This strong tumor suppression effect was also observed with another *dpn-RNAi* line that uses a different *dpn* targeting sequence (Figure S2A). In addition, knocking down *dpn* also abolished *ttk*-depletion-induced ectopic expression of other NB-specific factors, including Wor and m8 (Figures S2B–S2D).

Figure 1. *ttk*-Depleted ISCs Have Switched Their Self-Renewal Program into Neuroblast-like

(A) A schematic for the ISC lineage in adult *Drosophila* midgut. ISCs (marked by Dl) are able to self-renew and generate two types of committed progenitors—enteroblasts (EBs, marked by NRE-lacZ) and enteroendocrine progenitor cells (EEPs, marked by low levels of both Dl and Pros expression)—which, respectively, gives rise to enterocytes (ECs, marked by Pdm1) and enteroendocrine cells (EEs, marked by Pros). Esg marks all undifferentiated cells in the midgut epithelium, including ISCs, EBs, and EEPs.

(B–G) Representative superficial and cross-sectional views of *esg-GAL4,UAS-GAL80^{ts},UAS-GFP* in (B), (C), and (F) and *esg-GAL4,UAS-GAL80^{ts},UAS-GFP;UAS-ttk-IR* in (D), (E), and (G) adult *Drosophila* midguts. (B) and (D) show stained ISC marker Dl; (C) and (E) show stained EE marker Pros; and (F) and (G) show anti-Armadillo (Arm) staining. Arm is expressed at high levels specifically in ISCs and progenitor cells.

(H) Volcano plot showing the comparison of gene expression profiles of esg > GFP$^+$ cells without and with *ttk* depletion. Red dots depict genes that are highly upregulated in ttk-IR gut (log_2 fold change < 1; adjusted p 9 0.01), and green dots depict genes that are significantly downregulated in *ttk-IR* gut (log_2 fold change < −1; adjusted p 9 0.01). Black dots are representative of neural-specific genes.

(I) The GO analysis results for the significantly changed genes in *ttk-IR* tumor cells. The top 10 GO terms for the upregulated 1,887 genes are listed in red, and those for the downregulated 1,980 genes are listed in green. The size of the dot represents the number of genes in this GO term.

(J) The list of several NB-specific genes that are significantly upregulated as well as top 17 intestinal progenitor cell-specific genes that are significantly downregulated in *ttk*-depleted tumor cells.

(K–P) The ectopic expression of some NB-specific genes—including Dpn by anti-Dpn antibody staining (K and L), Wor by anti-Wor antibody staining (M and N), and m8 by m8-lacZ reporter expression (O and P)—is confirmed in *ttk*-depleted tumor cells. (K), (M), and (O) show images for *esg^{ts}>GFP*. (L), (N), and (P) show images for *esg^{ts}>GFP, ttk-IR*. Note that the ectopically expressed Dpn is mainly localized to the cell nucleus, but the ectopically expressed Wor appears to be cytoplasmic in most cells and nuclear in some GFP^{high} cells (arrows).

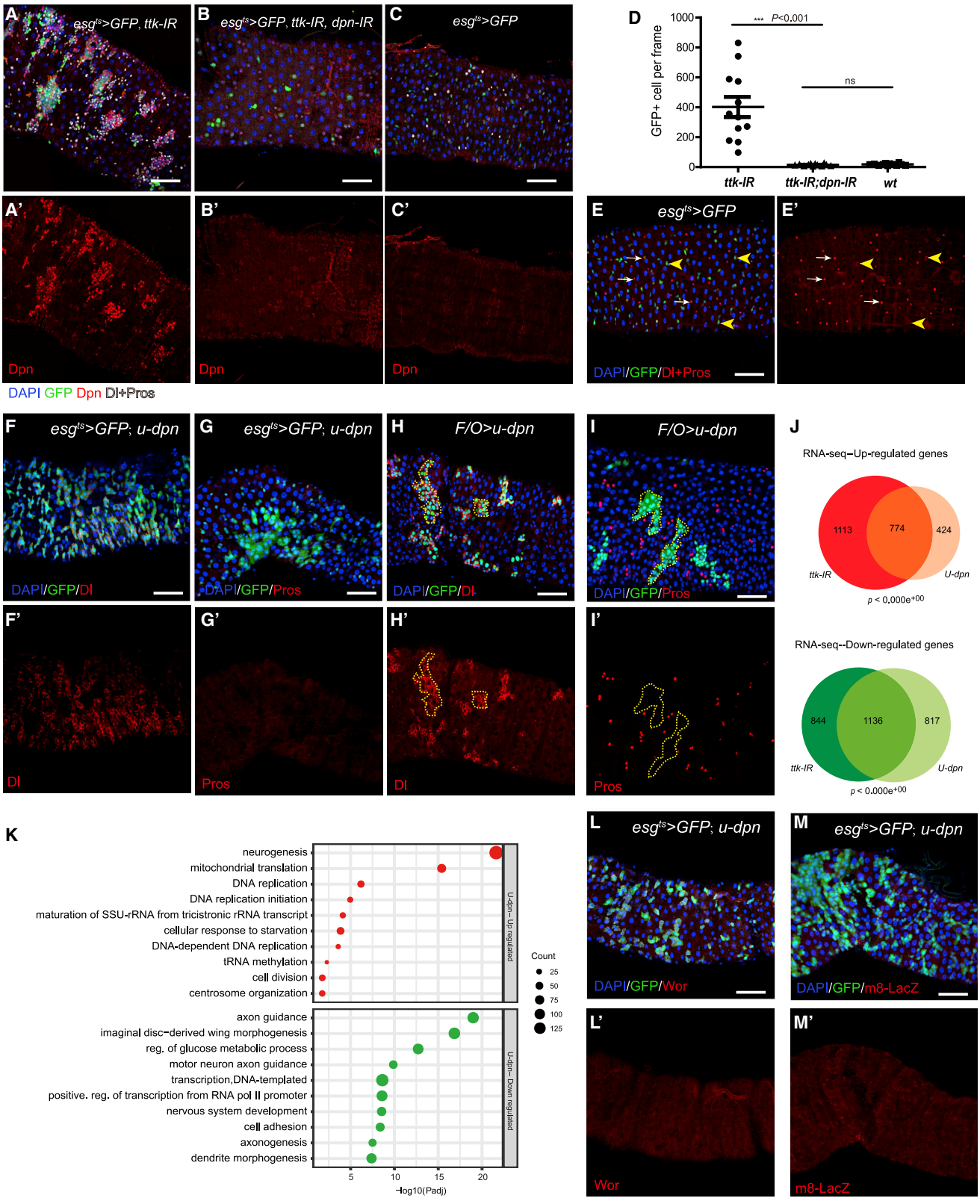

(legend on next page)

Dpn belongs to a member of HLH family transcription factors and is essential for viability. Its expression is relatively broad during early embryonic development, but it becomes largely confined to the central and periphery nervous at larval and adult stages, with no detectable expression in the digestive system (Bier et al., 1992; Robinson et al., 2013). Consistent with the notion that *dpn* expression is undetectable in the gut, depleting *dpn* generally in all ISCs or in induced clones did not cause any obvious effect on the proliferation or differentiation of ISCs (including the differentiation of EEs) (Figures S1B–S1D). Therefore, *dpn* is not required for the self-renewal of normal ISCs but is required for *ttk*-depleted ISCs.

Next, we asked whether the ectopic expression of *dpn* in normal ISCs is sufficient to generate NETs. Interestingly, the conditional expression of *dpn* for 7 days by *esg-GAL4^{ts}, UAS-dpn* caused massive ISC-like Dl$^+$ cell tumors to form, but EEs were eliminated from their epithelial tissues (Figures 2E–2G). We further analyzed the effect(s) of *dpn* overexpression in ISC clones that we induced using the FLP-out technique. Similarly, all of the GFP$^+$ clones overexpressing *dpn* developed into ISC-like small-cell tumors and did so in a cell-autonomous manner (Figure 2H). Of note, we observed that the clones only contained sporadic ECs but, again, did not contain any Pros$^+$ EEs (Figure 2I), suggesting that ectopic *dpn* expression enhanced ISC self-renewal so that cell differentiation is delayed or blocked.

We sorted out these *dpn*-overexpressed esg$^+$ cells from *esg-Gal4^{ts}, UAS-GFP, UAS-dpn* flies and performed gene expression analysis by RNA-seq. Interestingly, the global changes in gene expression caused by *dpn* overexpression were very similar to that caused by *ttk* depletion: there was a significant overlap in up- and downregulated genes between these two types of tumor cells (Figure 2J), and the top 10 up- and downregulated gene categories were also strikingly similar (Figure 2K). Therefore, ectopically expressed Dpn appears to be a major factor that drives self-renewal of *ttk*-depleted tumor cells.

Because *ttk*-depleted tumor cells continuously generate NE cells, but high *dpn* levels block cell differentiation, there must be another mechanism that promotes NE differentiation from these tumor cells, and this mechanism is likely not active in the tumor cells generated by *dpn* overexpression. In addition, overexpression of *dpn* failed to induce expression of other NB-specific genes, including *wor* and *E(spl)m8* (Figures 2L and 2M), further implying the involvement of other factors in *ttk*-depletion-induced NETs besides Dpn.

The Pan-neural Factor *Seq* Is a Direct Transcriptional Target of Ttk

We next used a targeted DNA adenine methyltransferase identification (DamID) method to identify potential Ttk targets by expressing a *Ttk69-Dam* fusion transgene. Ectopic expression of the *Ttk69-Dam* transgene in ISC clones inhibited clonal growth and caused suppression of EE specification, effects that are similar to that caused by Ttk transgene overexpression (Wang et al., 2015), indicating that the Ttk-Dam fusion gene is functional. We then extracted DNA from *esg>Ttk69-Dam* guts and performed DamID analysis. There were 3,187 genes with enriched Ttk-Dam peaks, but only 10.83% of these genes showed transcriptional upregulation following *ttk* depletion (Figure S2), indicating that the majority of upregulated genes is an indirect outcome of *ttk* depletion. Unexpectedly, the Ttk-Dam signal was absent from the *dpn* gene locus and from other NB-specific genes such as the *wor*, *m8*, and *mγ* gene loci, indicating that its role in suppressing the NB transcription program is also indirect (Figure S3). However, *sequoia* (*seq*), which encodes a pan-neuronally expressed zinc-finger transcription factor, showed Ttk-Dam binding peaks at about 5 kb upstream of its transcription start site (Figure S3). Staining with antibodies against Seq revealed strong expression in *ttk*-depleted tumor cells, while its expression was not detectable in wild-type intestine (Figures 3A and 3B). Thus, *seq* appears to be directly silenced by Ttk in ISCs.

Seq Promotes NE Differentiation and Is Required for the Ectopic Dpn Expression in *ttk*-Depleted Tumor Cells

Seq is an essential gene, and the encoded protein contains a DNA binding domain similar to that found in Ttk (Brenman et al., 2001; Gao et al., 1999). It has been reported to regulate terminal cell differentiation in the central nervous system and sensory organs (Andrews et al., 2009; Brenman et al., 2001; Gao et al., 1999). Therefore, *seq* could be responsible for the NE differentiation phenotype observed in *ttk*-depleted tumors. Indeed, co-depletion of *seq* completely suppressed the excessive EE

Figure 2. The Ectopic Dpn Expression Is Responsible for the Self-Renewal of *ttk*-Depleted ISCs

(A–D) Knocking down *dpn* (using RNAi line HMC03154) suppresses *ttk*-depletion-induced tumor.

(A–C) Representative images of the midguts of flies with *esg^{ts}>GFP, ttk-IR*; *esg^{ts}>GFP, ttk-IR, dpn-IR*; and *esg^{ts}>GFP*, respectively.

(D) Quantification of GFP$^+$ cells in areas of the same size (about 36,000 μm^2) from midguts of flies with the indicated genotypes. Data are presented as mean ± SEM; n = 12; p values by unpaired t test. ns, not significant.

(E–G) Overexpression of *dpn* for 7 days by *esg^{ts} > Gal4* in the progenitor cells generate Dl$^+$ cell tumor.

(E and E') Wild-type midgut stained with Dl (yellow arrowheads) and Pros (white arrows) antibodies.

(F and G) *Dpn*-overexpressed midgut stained with Dl (F) and Pros (G) antibodies. The clustered GFP$^+$ cells are strongly Dl$^+$.

(H and I) A FLP-out clone (marked by GFP, green) with *dpn* overexpression (*dpn-OE*) stained with Dl (H; red on membrane) and Pros (I; red in nuclear) antibodies. Dashed lines depict the clone margin.

(J) The left Venn diagram shows the overlap between the upregulated genes caused by *dpn* overexpression and those caused by *ttk* knockdown. The right Venn diagram shows the overlap between the downregulated genes caused by *dpn* overexpression and those caused by *ttk* knockdown. p values based on the hypergeometric distribution are shown.

(K) The GO analysis results for the significantly changed genes in *dpn-OE* tumor cells. The top 10 GO terms for the upregulated 1,198 genes are indicated in red and for the downregulated 1,953 genes are indicated in green; the size of the dot represents the number of genes in this GO term.

(L and M) The expressions of some NB-specific genes, including *m8-lacZ* (L) and *wor* (M), could not be detected in *dpn*-overexpressing tumor cells.

Scale bars, 50 μm.

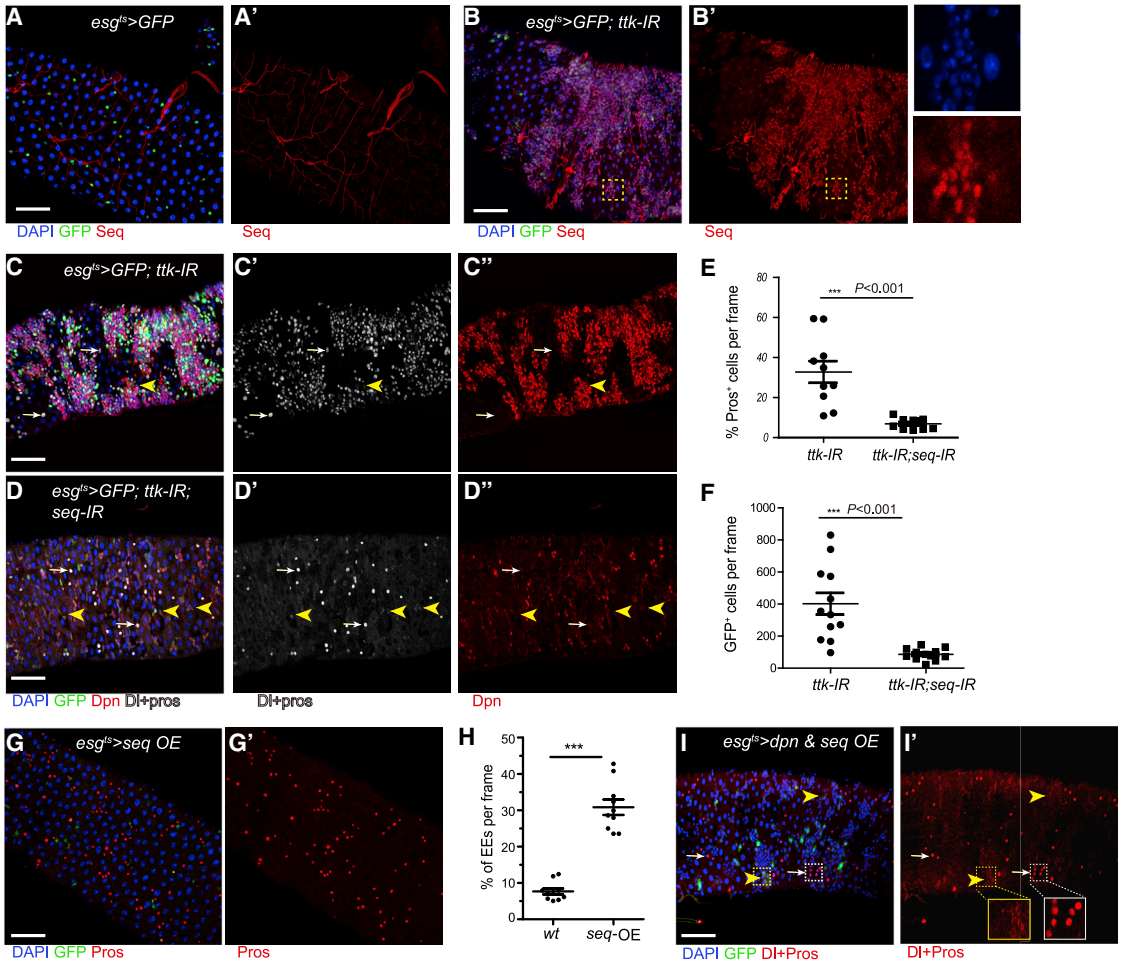

Figure 3. The Ectopic Dpn Expression in *ttk*-Depleted Cells Requires Seq, which Also Promotes NE Differentiation

(A and B) Seq shows ectopic expression in *ttk*-depleted tumor cells (B) but not in wild-type intestine (A); a zoomed-in frame shows the nucleus localization of Seq staining in (B).

(C–F) Knocking down *seq* suppresses *ttk*-depletion-induced *dpn* expression and tumorigenesis.

(C) and (D) show representative images of the midguts of *esg^{ts}>GFP;ttk-IR* and *esg^{ts}>GFP;ttk-IR;seq-IR* flies, respectively (yellow arrowheads indicate ISC marker Dl; white arrows indicate EE marker Pros).

(E) Quantification of the percentages of Pros$^+$ cells in *esg-GAL4,UAS-GAL80^{ts},UAS-GFP;UAS-ttk-IR* (*ttk-IR*) and *esg-GAL4,UAS-GAL80^{ts},UAS-GFP;UAS-ttk-IR;UAS-seq-IR (ttk-IR;seq-IR)* midguts. Data are presented as mean ± SEM; n = 10; p values by unpaired t test.

(F) The quantification of GFP$^+$ progenitor cells in *ttk-IR* and *ttk-IR;seq-IR* midguts. Data are presented as mean ± SEM; n = 12; p values by unpaired t test.

(G and H) Ectopic expression of Seq causes increased percentage of Pros$^+$ cells in the midgut.

(G) Representative images of *esg-GAL4,UAS-GAL80^{ts},UAS-GFP;UAS-seq (esg^{ts} > GFP, seq OE)* midguts.

(H) Quantification of the percentages of Pros$^+$ cells in control and *seq OE* midguts. Data are presented as mean ± SEM; n = 10; p values by unpaired t test.

(I) Co-expression of *seq* and *dpn* induces tumor with Pros$^+$ cells (white arrows) and Dl$^+$ cells (yellow arrowheads).

Scale bars, 50 μm.

phenotype following *ttk* depletion (Figures 3C–3F). In addition, forced expression of *seq* in esg$^+$ cells caused a significant increase in EEs in the intestinal epithelium (Figures 3G and 3H). Further, co-expression of *seq* allowed EE generation from *dpn*-induced ISC-like cells (Figure 3I), generating a NET-like phenotype. As *AS-C* genes are derepressed in *ttk*-depleted tumors and are responsible for the excessive EE phenotype (Wang et al., 2015), we next determined whether expression of *seq* was sufficient to induce *AS-C* gene expression. Indeed, using a sc-GFP knockin fusion reporter, we observed significantly increased sc-GFP expression in esg$^+$ cells caused by *seq* overexpression (data not shown). These observations collectively suggest that *seq* expression is sufficient to promote EE generation from both normal ISCs and *dpn*-induced ISC-like cells by promoting *AS-C* gene expression. Again, similar to the functional requirement of *dpn*, analysis of *seq* mutant clones demonstrated that *seq* is not required for EE generation from normal ISCs (Figure S1), showing that the *ttk*-depleted ISCs specifically require *seq* and *dpn* for their self-renewal and differentiation. Explicitly, *dpn* is essential for the self-renewal of *ttk*-depleted tumor cells,

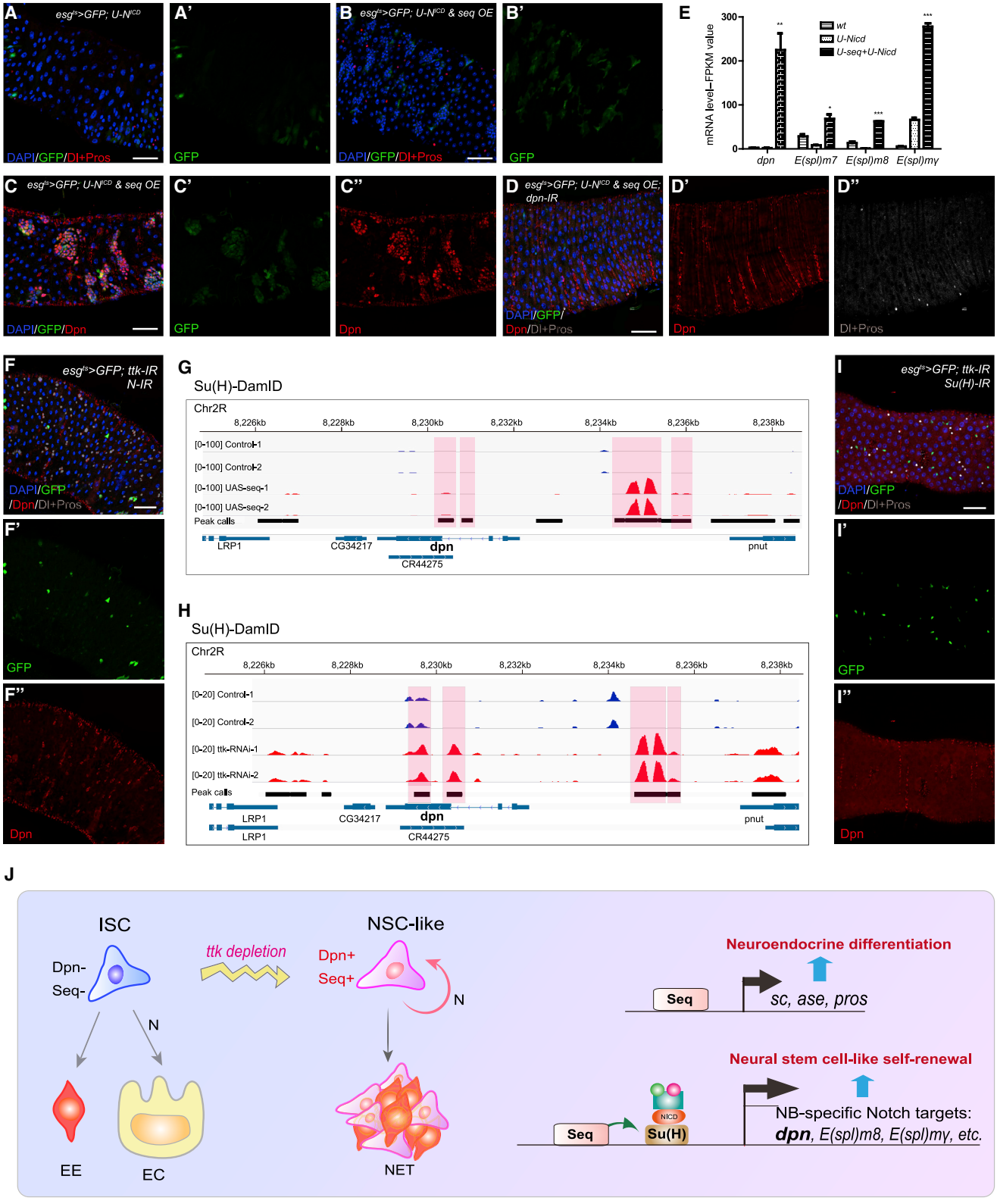

Figure 4. Seq Allows NB-Specific Genes Responsive to Notch in ISCs

(A and B) Representative images of esg-GAL4,UAS-GAL80^{ts},UAS-GFP;UAS-N^{icd} (A) and esg-GAL4,UAS-GAL80^{ts},UAS-GFP;UAS-N^{icd};UAS-seq (B) midguts. (C) Expression of Dpn (indicated by Dpn antibody in red) in the tumor cells of the *N^{icd} & seq OE* midgut.

(legend continued on next page)

while *seq* has an additional role in promoting NE differentiation from *ttk*-depleted tumor cells.

We found that depletion of *seq* also eliminated ectopic Dpn expression in *ttk*-depleted tumors (Figures 3C, 3D, and 3F), which not only explains the requirement of *seq* in tumor formation but also indicates that the expression of Dpn requires *seq*. However, overexpression of *seq* in ISCs is not sufficient to induce Dpn expression (data not shown), implying that Dpn expression in *ttk*-depleted tumor cells may require additional factors besides Seq.

Seq Inverts Differentiation-Promoting Function of Notch into a Self-Renewal Role

In NBs, Dpn is considered to be a transcriptional target of Notch (Babaoğlan et al., 2013; San-Juán and Baonza, 2011). Therefore, we asked whether Notch could serve as another factor along with Seq to induce Dpn expression and initiate NETs from ISCs. This idea is somewhat paradoxical, as it is known that Notch functions inversely in controlling the differentiation of ISCs and NBs: Notch activity is necessary for NB (type II) maintenance (and its overactivation induces NB overproliferation) (Bowman et al., 2008; Wang et al., 2006), while Notch activation in ISCs induces differentiation (Micchelli and Perrimon, 2006; Ohlstein and Spradling, 2006). We thus conducted experiments to determine whether the *seq*-overexpressed ISCs behave more similarly to ISCs than to NBs in response to Notch activation.

Similar to previous observations, we found that the conditional expression of the active form of Notch, N^{icd} (intracellular domain of Notch), was sufficient to cause ISC loss in the posterior midgut by promoting ISC differentiation into ECs (Figure 4A). Interestingly, the conditional expression of N^{icd} in *seq*-overexpressed ISCs not only failed to induce cell differentiation but also promoted the formation of small cell tumors (Figure 4B). These tumor cells were highly proliferative (Figures S4A–S4C). They had significantly reduced *esg>GFP* expression and did not show obvious Dl expression, but they also failed to generate terminally differentiated cells, except for the sporadic presence of some weak $Pros^{+}$ cells in the tumors (Figure 4B; Figures S4D–S4G), indicating that the majority of the tumor cells remained in an undifferentiated state. Co-activation of Notch was able to strongly induce Dpn expression in *seq*-overexpressed ISCs (Figure 4C), and this ectopic expression of Dpn was absolutely required for tumor development (Figures S4D–S4G). In addition to *dpn*, several other NB-specific genes, including *E(spl)m8* and *mγ*, were also activated following co-activation of Notch and Seq (Figure 4E). Therefore, *seq*-overexpressed ISCs behave similarly to NBs in response to Notch activation, and *seq* expression causes a shift in Notch's function—from promoting differentiation to promoting self-renewal by rendering NB-specific genes, such as *dpn*, responsive to Notch.

It is worth mentioning that the conditional expression of N^{icd} in *dpn*-overexpressed ISCs exhibited an ISC loss phenotype similar to that caused by N^{icd} overexpression alone (Figure S4H). Therefore, unlike Seq, ectopic Dpn expression in ISCs is not sufficient to switch Notch from promoting differentiation to promoting self-renewal, implying that Seq has additional targets, such as other NB-specific genes, some of which may act together with Dpn to fulfill this function.

As Dl expression is reduced in *ttk*-depleted tumor cells, the aforementioned results imply that there may be a low level of Notch activity in the tumor cells that cooperates with Seq to induce the expression of Dpn, thereby promoting tumor development. Consistent with this notion, co-depleting Notch in *ttk*-depleted ISCs strongly suppressed Dpn expression; consequently, the tumorigenesis was prevented (Figure 4F).

Seq Renders NB-Specific Genes Responsive to Notch

Previous studies have shown that *seq* and *Notch* mutant embryos share many similar phenotypes in the nervous system, indicating that *seq* could function in the Notch pathway (Andrews et al., 2009; Brenman et al., 2001; Gunnar et al., 2016). Seq protein contains two C2H2 zinc fingers at its middle region, which bind to DNA, and polyglutamine-rich repeats at its N and C termini (Brenman et al., 2001), which are believed to mediate protein-protein interactions. Given these sequence features, we speculate that Seq could have a role in facilitating Notch signaling at the chromatin level and, in this case, facilitating ectopic NB-specific gene activation by Notch in ISCs. To test this hypothesis, we performed DamID analysis of wild-type, *seq*-overexpressed, and *ttk*-depleted ISCs for the DNA-binding transcription factor Suppressor of Hairless (Su(H)), which mediates Notch signaling (Furriols and Bray, 2001; Morel et al., 2001). As predicted, the *seq*-overexpressed ISCs, as well as *ttk*-depleted ISCs, but not wild-type ISCs, showed significant Su(H)-Dam binding signals at the enhancer and gene coding regions of *dpn*, *m8*, and *mγ* (Figures 4G and 4H; Figure S5). Importantly, depleting Su(H) effectively suppressed *ttk*-depletion-induced Dpn activation; consequently, the NET formation was prevented (Figure 4I). Collectively, these data suggest that

(D) Knocking down *dpn* suppresses the tumor in N^{icd} *OE & seq OE* midgut.
(E) The mRNA levels of *dpn*, *E(spl)m7*, *E(spl)m8*, and *E(spl)mγ* in wild-type (wt), N^{icd} overexpressed (*U-Nicd*), and N^{icd} and *seq* co-overexpressed (*U-seq+U-Nicd*) progenitor cells by high-throughput sequencing. *$p < 0.05$; **$p < 0.01$;***$p < 0.001$. Three independent biological replicates were performed.
(F) Co-depleting *Notch* suppresses ectopic Dpn expression and tumor formation in *ttk-IR* midgut.
(G and H) Su(H)-Dam binding profiles for *dpn* loci (blocked in black) in normal (blue peaks) and *seq*-overexpressed (red peaks) progenitor cells. Intensity range: 0–100. Black and pink boxes indicate Su(H) binding sites that are enriched in *seq*-overexpressed (G) or *ttk*-depleted (H) midguts compared with normal midguts (fold change > 2; adjusted $p < 0.01$). Associated genes or transcripts are indicated in blue.
(I) Co-depleting *su(H)* suppresses ectopic Dpn expression and tumor formation in *ttk-IR* midgut.
(J) A model of NET tumor development from *ttk*-depleted ISCs. Loss of Ttk causes an ISC-to-NSC self-renewal program switch and NET tumorigenesis. Loss of Ttk causes derepression of Seq, which induces the functional switch of Notch by rendering NB-specific genes—*dpn*, in particular—responsive to Notch activation, thereby inverting the differentiation-promoting function of Notch into a self-renewal role. Seq also promotes NE differentiation by activating the AS-C-Pros regulatory axis. The cooperative activity of Seq and Dpn drives NET tumorigenesis from *ttk*-depleted ISCs.
Scale bars, 50 μm.

the presence of Seq allowed the recruitment of Su(H) to the enhancers of NB-specific genes that are normally silenced in ISCs, thereby rendering these genes responsive to Notch activation. Therefore, Seq has a "selector" function in ISCs whose expression allows NB-specific genes to be expressed via Notch activation and, thus, inverts the differentiation-promoting function of Notch into a self-renewal role as in normal NSCs.

DISCUSSION

Our results reveal an ISC-to-NB switch in the tissue stem cell self-renewal program that drives NET development from *ttk*-depleted ISCs. Loss of *ttk* causes the derepression of NB-specific transcription factors, including *dpn* and *seq*, and the concomitant loss of ISC-specific factors. The ectopically expressed Dpn acts as a major self-renewal factor for the self-duplication of tumor cells, while Seq has a "selector" function in selecting Notch target genes by recruiting Su(H) to the enhancer regions of NB-specific genes, thereby rendering these genes responsive to Notch in the tumor cells. In addition, Seq also has a role in NE differentiation by inducing *AS-C* gene expression. The cooperative function of Dpn and Seq leads to the activation of a NB-like self-renewal program as well as a NE differentiation program and the continuous activation of these two programs leading to NET development from ISCs (Figure 4J).

There are two types of NBs in the central brain of *Drosophila* larva: type I and type II. Dpn is expressed in both types of NBs, but the type II NBs are more sensitive to the changes of Dpn; interestingly, the type II NBs are more sensitive to the changes of Notch signaling as well (San-Juán and Baonza, 2011). Thus, it appears that the ectopically activated self-renewal program in ISCs described here is more similar to that used in the type II NBs. Compared to the type I NB lineage, the type II NB lineage goes through one extra type of transient amplification progenitors before terminal cell fate specification (Homem and Knoblich, 2012), indicating that this type II-like self-renewal program, if hijacked by tumor cells, could potentially be more potent to initiate tumorigenesis.

As the loss of a single factor, Ttk, in ISCs is sufficient for the switch of tissue stem cell program and for the subsequent development of NETs in the midgut, Ttk could be viewed as a specific class of stem cell factors, which we propose here as a tissue identity maintenance (TIM) factor; such factors function to safeguard the tissue identity of stem cells. ISCs not only give rise to ECs that function to digest and absorb nutrients but also give rise to neural-like EE cells. Conceivably, ISCs may need to use a basal or transient neural-like program in order to endow their capacity to generate EEs, as the proneural factor Sc is transiently expressed in ISCs, and this transient expression initiates EE generation (Chen et al., 2018; Yin and Xi, 2018). In this context, a stem cell identity factor like Ttk may be necessary to enable ISCs to maintain a gut identity and thereby prevent excessive acquisition of NSC-like traits.

The Ttk protein is characterized by having a BTB domain in addition to a zinc-finger DNA-binding domain, and although there is no direct protein ortholog of Ttk in mammals, BTB-domain-containing transcription factors are found in all eukaryotes, including mammals (Perez-Torrado et al., 2006). Moreover, alteration of Notch activity as well as increased expression of proneural genes are also known to occur in mammalian models of NETs and in human NETs (Balanis et al., 2019; Ball, 2004; Crabtree et al., 2016; Park et al., 2018). Thus, it is possible that there are TIM factors that function in stem cells in other tissues and organisms and that "stem cell identity switch" could be a common mechanism underlying NET formation and, possibly, other stem-cell-mediated tumorigenesis.

STAR★METHODS

Detailed methods are provided in the online version of this paper and include the following:

- KEY RESOURCES TABLE
- LEAD CONTACT AND MATERIALS AVAILABILITY
- EXPERIMENTAL MODEL AND SUBJECT DETAILS
  - Fly Stocks and Cultivation
- METHOD DETAILS
  - Generation of DamID Transgenic Flies
  - Immunohistochemistry and Microscopy
  - Cryosectioning
  - Fluorescence-Activated Cell Sorting (FACS), RNA isolation, and Amplification
  - RNA Sequencing and Data Analysis
  - DamID Sequencing and Data Analysis
- QUANTIFICATION AND STATISTICAL ANALYSIS
- DATA AND CODE AVAILABILITY

SUPPLEMENTAL INFORMATION

Supplemental Information can be found online at https://doi.org/10.1016/j.celrep.2020.01.041.

ACKNOWLEDGMENTS

We thank the members of the fly community, as cited in STAR Methods, for generously providing reagents; the Bloomington Drosophila Stock Center (BDSC), the Tsinghua Fly Center, the Vienna Drosophila RNAi Center (VDRC), and the Development Studies Hybridoma Bank (DSHB) for reagents; Dr. John Snyder for editing the manuscript; and the Xi lab members for discussions. This work was supported by a National Key Research and Development Program of China grant (2017YFA0103602) and a National Basic Research Program of China (2014CB850002) grant from from the Chinese Ministry of Science and Technology.

AUTHOR CONTRIBUTIONS

Z.L., X.G., and R.X. designed the experiments. Z.L., X.G., C.W., F.Y., and L.H. performed the experiments. H.H., Y.Z., J.W., and T.C. performed the informatics analysis. Z.J. helped with data analysis and figure preparation. R.X. acquired funding. Z.L., X.G., H.H., and R.X. wrote the paper.

DECLARATION OF INTERESTS

The authors declare no competing interests.

Received: July 22, 2019
Revised: November 15, 2019
Accepted: January 13, 2020
Published: February 11, 2020; corrected online December 1, 2020

REFERENCES

Andrews, H.K., Giagtzoglou, N., Yamamoto, S., Schulze, K.L., and Bellen, H.J. (2009). Sequoia regulates cell fate decisions in the external sensory organs of adult *Drosophila*. EMBO Rep. *10*, 636–641.

Babaoğlan, A.B., Housden, B.E., Furriols, M., and Bray, S.J. (2013). Deadpan contributes to the robustness of the notch response. PLoS ONE *8*, e75632.

Balanis, N.G., Sheu, K.M., Esedebe, F.N., Patel, S.J., Smith, B.A., Park, J.W., Alhani, S., Gomperts, B.N., Huang, J., Witte, O.N., and Graeber, T.G. (2019). Pan-cancer convergence to a small-cell neuroendocrine phenotype that shares susceptibilities with hematological malignancies. Cancer Cell *36*, 17–34.e7.

Ball, D.W. (2004). Achaete-scute homolog-1 and Notch in lung neuroendocrine development and cancer. Cancer Lett. *204*, 159–169.

Berger, C., Harzer, H., Burkard, T.R., Steinmann, J., van der Horst, S., Laurenson, A.S., Novatchkova, M., Reichert, H., and Knoblich, J.A. (2012). FACS purification and transcriptome analysis of *Drosophila* neural stem cells reveals a role for Klumpfuss in self-renewal. Cell Rep. *2*, 407–418.

Bier, E., Vaessin, H., Younger-Shepherd, S., Jan, L.Y., and Jan, Y.N. (1992). *deadpan*, an essential pan-neural gene in *Drosophila*, encodes a helix-loop-helix protein similar to the *hairy* gene product. Genes Dev. *6*, 2137–2151.

Biteau, B., and Jasper, H. (2014). Slit/Robo signaling regulates cell fate decisions in the intestinal stem cell lineage of *Drosophila*. Cell Rep. *7*, 1867–1875.

Bowman, S.K., Rolland, V., Betschinger, J., Kinsey, K.A., Emery, G., and Knoblich, J.A. (2008). The tumor suppressors Brat and Numb regulate transit-amplifying neuroblast lineages in *Drosophila*. Dev. Cell *14*, 535–546.

Brand, A.H., and Perrimon, N. (1993). Targeted gene expression as a means of altering cell fates and generating dominant phenotypes. Development *118*, 401–415.

Brenman, J.E., Gao, F.B., Jan, L.Y., and Jan, Y.N. (2001). Sequoia, a Tramtrack-related zinc finger protein, functions as a pan-neural regulator for dendrite and axon morphogenesis in *Drosophila*. Dev. Cell *1*, 667–677.

Campuzano, S., and Modolell, J. (1992). Patterning of the *Drosophila* nervous system: the *achaete-scute* gene complex. Trends Genet. *8*, 202–208.

Chen, J., Xu, N., Huang, H., Cai, T., and Xi, R. (2016). A feedback amplification loop between stem cells and their progeny promotes tissue regeneration and tumorigenesis. eLife *5*, e14330.

Chen, J., Xu, N., Wang, C., Huang, P., Huang, H., Jin, Z., Yu, Z., Cai, T., Jiao, R., and Xi, R. (2018). Transient Scute activation via a self-stimulatory loop directs enteroendocrine cell pair specification from self-renewing intestinal stem cells. Nat. Cell Biol. *20*, 152–161.

Crabtree, J.S., Singleton, C.S., and Miele, L. (2016). Notch signaling in neuroendocrine tumors. Front. Oncol. *6*, 94.

de Navascués, J., Perdigoto, C.N., Bian, Y., Schneider, M.H., Bardin, A.J., Martínez-Arias, A., and Simons, B.D. (2012). *Drosophila* midgut homeostasis involves neutral competition between symmetrically dividing intestinal stem cells. EMBO J. *31*, 2473–2485.

Doupé, D.P., Marshall, O.J., Dayton, H., Brand, A.H., and Perrimon, N. (2018). *Drosophila* intestinal stem and progenitor cells are major sources and regulators of homeostatic niche signals. Proc. Natl. Acad. Sci. USA *115*, 12218–12223.

Dutta, D., Xiang, J., and Edgar, B.A. (2013). RNA expression profiling from FACS-isolated cells of the *Drosophila* intestine. Curr. Protoc. Stem Cell Biol. *27*, Unit 2F.2.

Furriols, M., and Bray, S. (2001). A model Notch response element detects Suppressor of Hairless-dependent molecular switch. Curr. Biol. *11*, 60–64.

Gao, F.B., Brenman, J.E., Jan, L.Y., and Jan, Y.N. (1999). Genes regulating dendritic outgrowth, branching, and routing in *Drosophila*. Genes Dev. *13*, 2549–2561.

Ghysen, A., Dambly-Chaudière, C., Jan, L.Y., and Jan, Y.N. (1993). Cell interactions and gene interactions in peripheral neurogenesis. Genes Dev. *7*, 723–733.

Gunnar, E., Bivik, C., Starkenberg, A., and Thor, S. (2016). *sequoia* controls the type I>0 daughter proliferation switch in the developing *Drosophila* nervous system. Development *143*, 3774–3784.

Guo, X., Huang, H., Yang, Z., Cai, T., and Xi, R. (2019a). Division of labor: roles of Groucho and CtBP in Notch-mediated lateral inhibition that controls intestinal stem cell differentiation in *Drosophila*. Stem Cell Reports *12*, 1007–1023.

Guo, X., Yin, C., Yang, F., Zhang, Y., Huang, H., Wang, J., Deng, B., Cai, T., Rao, Y., and Xi, R. (2019b). The cellular diversity and transcription factor code of Drosophila enteroendocrine cells. Cell Rep. *29*, 4172–4185.e5.

Gutierrez-Triana, J.A., Mateo, J.L., Ibberson, D., Ryu, S., and Wittbrodt, J. (2016). iDamIDseq and iDEAR: an improved method and computational pipeline to profile chromatin-binding proteins. Development *143*, 4272–4278.

Homem, C.C., and Knoblich, J.A. (2012). *Drosophila* neuroblasts: a model for stem cell biology. Development *139*, 4297–4310.

Hung, R., Kirchner, Y.H.R., Li, F., Xu, C., Comjean, A., Tattikota, S., Song, W., Sui, S., and Perrimon, N. (2018). A cell atlas of the adult *Drosophila* midgut. bioRxiv. https://doi.org/10.1101/410423.

Korzelius, J., Naumann, S.K., Loza-Coll, M.A., Chan, J.S., Dutta, D., Oberheim, J., Gläßer, C., Southall, T.D., Brand, A.H., Jones, D.L., and Edgar, B.A. (2014). *Escargot* maintains stemness and suppresses differentiation in *Drosophila* intestinal stem cells. EMBO J. *33*, 2967–2982.

Lan, Q., Cao, M., Kollipara, R.K., Rosa, J.B., Kittler, R., and Jiang, H. (2018). FoxA transcription factor Fork head maintains the intestinal stem/progenitor cell identities in *Drosophila*. Dev. Biol. *433*, 324–343.

Lee, T., and Luo, L. (1999). Mosaic Analysis with a Repressible Cell Marker for Studies of Gene Function in Neuronal Morphogenesis. Neuron *22*, 451–461.

Lin, G., Xu, N., and Xi, R. (2008). Paracrine Wingless signalling controls self-renewal of *Drosophila* intestinal stem cells. Nature *455*, 1119–1123.

Loza-Coll, M.A., Southall, T.D., Sandall, S.L., Brand, A.H., and Jones, D.L. (2014). Regulation of *Drosophila* intestinal stem cell maintenance and differentiation by the transcription factor Escargot. EMBO J. *33*, 2983–2996.

McGuire, S.E., Mao, Z., and Davis, R.L. (2004). Spatiotemporal Gene Expression Targeting with the TARGET and Gene-Switch Systems in Drosophila. Sci. STKE. *220*, pl6.

Meng, F.W., and Biteau, B. (2015). A Sox transcription factor is a critical regulator of adult stem cell proliferation in the *Drosophila* intestine. Cell Rep. *13*, 906–914.

Micchelli, C.A., and Perrimon, N. (2006). Evidence that stem cells reside in the adult *Drosophila* midgut epithelium. Nature *439*, 475–479.

Morel, V., Lecourtois, M., Massiani, O., Maier, D., Preiss, A., and Schweisguth, F. (2001). Transcriptional repression by suppressor of hairless involves the binding of a hairless-dCtBP complex in *Drosophila*. Curr. Biol. *11*, 789–792.

Nässel, D.R., and Winther, A.M. (2010). *Drosophila* neuropeptides in regulation of physiology and behavior. Prog. Neurobiol. *92*, 42–104.

Ohlstein, B., and Spradling, A. (2006). The adult *Drosophila* posterior midgut is maintained by pluripotent stem cells. Nature *439*, 470–474.

Ohlstein, B., and Spradling, A. (2007). Multipotent *Drosophila* intestinal stem cells specify daughter cell fates by differential notch signaling. Science *315*, 988–992.

Oronsky, B., Ma, P.C., Morgensztern, D., and Carter, C.A. (2017). Nothing but NET: a review of neuroendocrine tumors and carcinomas. Neoplasia *19*, 991–1002.

Park, J.W., Lee, J.K., Sheu, K.M., Wang, L., Balanis, N.G., Nguyen, K., Smith, B.A., Cheng, C., Tsai, B.L., Cheng, D., et al. (2018). Reprogramming normal human epithelial tissues to a common, lethal neuroendocrine cancer lineage. Science *362*, 91–95.

Perez-Torrado, R., Yamada, D., and Defossez, P.A. (2006). Born to bind: the BTB protein-protein interaction domain. BioEssays *28*, 1194–1202.

Robinson, S.W., Herzyk, P., Dow, J.A., and Leader, D.P. (2013). FlyAtlas: database of gene expression in the tissues of *Drosophila melanogaster*. Nucleic Acids Res. *41*, D744–D750.

San-Juán, B.P., and Baonza, A. (2011). The bHLH factor *deadpan* is a direct target of Notch signaling and regulates neuroblast self-renewal in *Drosophila*. Dev. Biol. *352*, 70–82.

Southall, T.D., Gold, K.S., Egger, B., Davidson, C.M., Caygill, E.E., Marshall, O.J., and Brand, A.H. (2013). Cell-type-specific profiling of gene expression and chromatin binding without cell isolation: assaying RNA Pol II occupancy in neural stem cells. Dev. Cell *26*, 101–112.

Wang, H., Somers, G.W., Bashirullah, A., Heberlein, U., Yu, F., and Chia, W. (2006). Aurora-A acts as a tumor suppressor and regulates self-renewal of *Drosophila* neuroblasts. Genes Dev. *20*, 3453–3463.

Struhl, G., and Basler, K. (1993). Organizing activity of wingless protein in Drosophila. Cell *72*, 527–540.

Wang, C., Guo, X., Dou, K., Chen, H., and Xi, R. (2015). Ttk69 acts as a master repressor of enteroendocrine cell specification in *Drosophila* intestinal stem cell lineages. Development *142*, 3321–3331.

Yin, C., and Xi, R. (2018). A phyllopod-mediated feedback loop promotes intestinal stem cell enteroendocrine commitment in *Drosophila*. Stem Cell Reports *10*, 43–57.

Zacharioudaki, E., Magadi, S.S., and Delidakis, C. (2012). bHLH-O proteins are crucial for *Drosophila* neuroblast self-renewal and mediate Notch-induced overproliferation. Development *139*, 1258–1269.

Zeng, X., and Hou, S.X. (2015). Enteroendocrine cells are generated from stem cells through a distinct progenitor in the adult *Drosophila* posterior midgut. Development *142*, 644–653.

Zhai, Z., Kondo, S., Ha, N., Boquete, J.P., Brunner, M., Ueda, R., and Lemaitre, B. (2015). Accumulation of differentiating intestinal stem cell progenies drives tumorigenesis. Nat. Commun. *6*, 10219.

Zhai, Z., Boquete, J.P., and Lemaitre, B. (2017). A genetic framework controlling the differentiation of intestinal stem cells during regeneration in *Drosophila*. PLoS Genet. *13*, e1006854.

STAR★METHODS

KEY RESOURCES TABLE

REAGENT or RESOURCE	SOURCE	IDENTIFIER
Antibodies		
mouse monoclonal anti-Dl	The Developmental Studies Hybridoma Bank	Cat#C594.9B; RRID:AB_528194
mouse monoclonal anti-Pros	The Developmental Studies Hybridoma Bank	Cat#MR1A; RRID:AB_528440
rabbit anti-Dpn	gift from Yuh-Nung Jan, UCSF, USA	RRID:AB_2567048
rabbit anti-Seq	gift from Yuh-Nung Jan, UCSF, USA	RRID:AB_2567124
rabbit polyclonal anti-β-galactosidase	MP Biomedicals	Cat# 0855976; RRID:AB_2334934
mouse anti-Armadillo	The Developmental Studies Hybridoma Bank	Cat#N2 7A1; RRID:AB_528089
rabbit polyclonal anti-phospho-Histone H3	Cell Signaling Technology	Cat# 9701; RRID:AB_331535
rat anti-Wor	Abcam	Cat# ab196362
rabbit polyclonal anti-Pdm1	gift from Xiaohang Yang, Zhejiang University, China	N/A
rabbit monoclonal anti-GFP	Cell Signaling Technology	Cat #2956; RRID:AB_1196615
Chemicals, Peptides, and Recombinant Proteins		
DAPI	ThermoFisher	Cat#D1306; RRID:AB_2629482
Elastase	Sigma	Cat#: E0258
propidium iodide (PI)	Invitrogen	Cat#: P3566
Critical Commercial Assays		
Arcturus PicoPureTM RNA isolation kit	ThermoFisher Scientific	Cat#KIT0204
ArcturusTM RiboAmpTM HS PLUS RNA amplification kit	ThermoFisher Scientific	Cat# KIT0525
NEB Next Ultra II DNA library prep kits	New England Biolabs	Cat#: E7645L
Agilent high-sensitivity DNA kit	Agilent Technologies	Cat#: 5067-1513
Qubit dsDNA HS assay kit	Thermo Fisher Scientific	Cat#: Q32851
Illumina library quantification kit	Kapa Biosystems	Cat#: KK4824
Deposited Data		
All raw and processed RNA-seq and DamID datasets	This paper	GEO: GSE130943
Experimental Models: Organisms/Strains		
esg-Gal4, UAS-GFP	Gift from Shigeo. Hayashi, RIKEN Center for Developmental Biology, Japan	N/A
UAS-ttk-RNAi#1	Vienna Drosophila Resource Center	VDRC: 10855, GD4414
UAS-Notch-RNAi	BDSC	7078
UAS-Nicd	Gift from Ting Xie, Stowers Institute for Medical Research, USA	N/A
UAS-dpn	This study	N/A
UAS-dpn.ORF.3xHA.GW	FlyORF	FlyORF: F000086, Flybase: FBst0501311
Gbe-Su(H)m8-lacZ (NRE-lacZ)	(Furriols and Bray, 2001)	N/A
seq^{vr5-5}	Bloomington Drosophila Stock Center	BDSC:5559, Flybase: FBst0005559
UAS-seq	Bloomington Drosophila Stock Center	BDSC:9244, Flybase: FBst0009244
m8-lacZ	Bloomington Drosophila Stock Center	BDSC:26786
UAS-seq-RNAi	Bloomington Drosophila Stock Center	BDSC:51923, Flybase: FBst0051923
UAS-dpn-RNAi #1	Bloomington Drosophila Stock Center	HMC03154, Flybase: FBst0051440
UAS-dpn-RNAi #2	Bloomington Drosophila Stock Center	JF02094, Flybase: FBst0026320

(*Continued on next page*)

Continued

REAGENT or RESOURCE	SOURCE	IDENTIFIER
sc-GFP	(Chen et al., 2018)	N/A
UAS-LT3-NDam	This study	N/A
UAS- LT3-NDam- Su(H)	This study	N/A
UAS-oDam	This study	N/A
UAS-ttk69-oDam	This study	N/A
UAS-seq-oDam	This study	N/A
Oligonucleotides		
cgGAATTCcaaacatgaagaagaacaggg	oDam-F	For generating UAS-oDam-attB-pUAST vector
CCGCTCGAGTTACGCGGCTGCACTTCCAC	oDam-R	For generating UAS-oDam-attB-pUAST vector
CCGCTCGAGATGAAGATGGCATCTCAACGC	Ttk-F	For generating UAS-ttk-oDam-attB-pUAST vector
GCTCTAGATTACTGCGCCGCAGCTGCTG	Ttk-R	For generating UAS-ttk-oDam-attB-pUAST vector
CCGCTCGAGATGCAACAATCGCGTAAATTTG	Seq-F	For generating UAS-seq-oDam-attB-pUAST vector
GCTCTAGATCAGAGAGCTAATAGCACTGCC	Seq-R	For generating UAS-seq-oDam-attB-pUAST vector
CCGCTCGAGATGAAGAGCTACAGCCAATTT	Su(H)-F	For generating UAS-Su(H)-TADam-attB-pUAST vector
GCTCTAGATCAGGATAAGCCGCTACCATG	Su(H)-R	For generating UAS-Su(H)-TADam-attB-pUAST vector
CTAATACGACTCACTATAGGGC AGCGTGGTCGCGGCCGAGGA	AdRt	5′-adaptor
TCCTCGGCCG	AdRb	3′-adaptor
GGTCGCGGCCGAGGATC	AdR_PCR	Amplification primer
Recombinant DNA		
Plasmid: pUASTattB-LT3-NDam	(Southall et al., 2013)	N/A
Plasmid: pCS2 oDam_f_GFPoNLS	(Gutierrez-Triana et al., 2016)	N/A
Plasmid: attB-pUAST-oDam	This study	N/A
Plasmid: UASTattB-LT3-NDam-Su(H)	This study	N/A
Plasmid: attB-pUAST-oDam-seq	This study	N/A
Plasmid: attB-pUAST-oDam-ttk69	This study	N/A
Software and Algorithms		
ImageJ	National Institutes of Health	https://imagej.net/Welcome
Prism	GraphPad	https://www.graphpad.com/scientific-software/prism/
Adobe Photoshop CS5	Adobe	https://www.adobe.com/uk/products/photoshop.html
Adobe Illustrator CC 2014	Adobe	https://adobe.com/uk/products/illustrator.html
Nikon Confocal Software	Nikon	https://www.microscope.healthcare.nikon.com/products/software/nis-elements/nis-elements-confocal
R package iDEAR 2.0	(Gutierrez-Triana et al., 2016)	https://bitbucket.org/juanlmateo/idear

LEAD CONTACT AND MATERIALS AVAILABILITY

Further information and requests for resources and reagents should be directed to and will be fulfilled by the Lead Contact, Rongwen Xi (xirongwen@nibs.ac.cn). All unique reagents generated in this study are available from the Lead Contact without restriction.

EXPERIMENTAL MODEL AND SUBJECT DETAILS

Fly Stocks and Cultivation

Animal care and use followed the institutional guidelines of the National Institute of Biological Sciences (NIBS), Beijing, and the authors affirm that the study is compliant with all relevant ethical regulations regarding animal research.

Flies were cultured on standard media under cultivation temperature of 25°C unless otherwise noted. All strains used in this study were listed in the Key Resources Table. The GAL4/UAS/GAL80^{ts} system was used for gene depletion and overexpression (OE) (Brand and Perrimon, 1993; McGuire et al., 2004). esg-GAL4, UAS-GFP; Tub-GAL80ts flies were crossed at 18°C to UAS-RNAi or UAS-OE transgenic flies. 3-5 days after eclosion, the female flies of the desired genotype were shifted to 29°C to inactivate GAL80ts and induce GAL4-mediated expression. Midguts were generally collected for immunostaining 5-7 days after shifting to 29°C, unless specified in the figure caption or legend. The crosses for FLP-out (Struhl and Basler, 1993) and MARCM analysis (Lee and Luo, 1999) were performed at 25°C. The female flies with desired genotype were heat-shocked at 37°C for 1 hour after 3-5 days of eclosion and then cultured on corn meal supplied with yeast paste for 5-7 days before dissection.

METHOD DETAILS

Generation of DamID Transgenic Flies

The pUASTattB-LT3-NDam-Su(H) vector was generated by inserting the CDS region of Su(H) into the multiple cloning site of pUAS-TattB-LT3-NDam vector (a gift from Andrea H. Brand, University of Cambridge, UK) (Southall et al., 2013); attB-pUAST-oDam was obtained by inserting the oDam sequence (amplified from pCS2 oDam_f_GFPoNLS vector (a gift from Jose Arturo Gutierrez-Triana, University of Heidelberg) (Gutierrez-Triana et al., 2016) by PCR) into the multiple cloning site of attB-pUAST vector. Then the attB-pUAST-oDam vector was used to generate attB-pUAST-oDam-ttk69 and attB-pUAST-oDam-Seq vectors. All the plasmids were purified using a QIAGEN Plasmid Midi Kit (#12145) and verified by sequencing. The transgenes were inserted into attP40 and attP2 sites using the phiC31 system via a standard microinjection protocol. For the generation of UAS-*dpn* transgenic fly, the cDNA of *dpn* was amplified by PCR from a *Drosophila* cDNA library and cloned into the pUAST vector followed by P-element-mediated transformation via a standard microinjection protocol.

Immunohistochemistry and Microscopy

Drosophila midgut were fixed, immunostained, and mounted as previously described (Lin et al., 2008). Briefly, 10-15 midguts of adult female flies were dissected in PBS and fixed at room temperature for 30 min using 4% paraformaldehyde, followed by dehydration in methanol (for 5min) and rehydration in PBT solution (PBS containing 0.1% Triton X-100). Primary antibodies were incubated with samples in 5% NGS-PBT solution overnight at 4°C or 2h at room temperature. After washing three times using PBT, secondary antibodies were incubated at room temperature for 2 hours, followed by 5 min DAPI staining, and 70% glycerol was used to mount the samples. Primary antibodies used in this study were listed in the Key Resource Table. Secondary antibodies used in this studies were Alexa Fluor 488-, 568- or Cy5-conjugated goat anti-rabbit, anti-mouse or anti-rat IgGs (Molecular Probes, A11034-A11036, A10524; 1:300). Nuclei were stained with DAPI (Sigma-Aldrich, 1 μg/ml). Images of midguts were captured using Nikon A1 or Leica SP8 confocal microscopes. All acquired images were adjusted and assembled in Adobe Photoshop and Illustrator. Scale bars indicate 50 μm unless otherwise noted.

Cryosectioning

The pre-stained midguts were placed horizontally at the bottom of a small flat embedding mold (PELCO, Prod No.106), then covered with a layer of O.C.T. Compound (Tissue-Tek,4583) and frozen in −80°C. 10-20 μm cross-sections were generated at −20°C by a Microm HM525 cryostat. The sections were placed onto the poly-lysine (sigma)-coated slides (Citoglas) using a brush and dried at room temperature for 30-60min. Then the sections were rinsed twice with PBT and mounted with 75% glycerol.

Fluorescence-Activated Cell Sorting (FACS), RNA isolation, and Amplification

The RNA expression profiling of progenitor cells from indicated genotypes was performed according to a previously described protocol (Dutta et al., 2013; Guo et al., 2019a). Briefly, 100-150 female guts were dissected into ice-cold diethyl pyrocarbonate (DEPC)-treated PBS, and digested with elastase solution (Sigma, cat. no. E0258, 1mg/ml final concentration) at 25°C for 1 hr with shaking at 34 x g, during which the sample was pipetting up and down 30-40 times every 15 min for full dissociation. Dissociated samples were centrifuged at 300 g for 20 min at 4°C, re-suspended in 500 μL DEPC-PBS with 1mg/ml propidium iodide (PI, Invitrogen, P3566), filtered with 40 μm filters (BD Falcon) and sorted using a FACS Aria II sorter (BD Biosciences). PI-negative and GFP-positive cells in the midguts of *esg^{ts} > GFP* flies, *esg^{ts} > GFP; ttk-IR* flies, *esg^{ts} > GFP;U-dpn* flies, *esg^{ts} > GFP, U-N^{icd}* flies, *esg^{ts} > GFP;U-seq* flies and *esg^{ts} > GFP,U-N^{icd};U-seq* flies, which had been shifted to 29°C for 5-7 days, were sorted into 500 μL of RNA extraction buffer (from Arcturus PicoPure RNA isolation kit, Applied Biosystems, Cat#KIT0204), using w1118 midguts to set the fluorescence gate. For each of the three biological replicates, about 10,000 cells were sorted, the sorted samples were then incubated in 42°C for 1 hr and centrifuged 4min at 3000 x g at 4°C. The supernatant was transferred into 500 μL 70% RNase-free ethanol and mixed well. The following steps were performed using the Arcturus PicoPure RNA isolation kit based on the manufacturer's instructions with the

DNase I digestion step. The RNA was then amplified using an Arcturus RiboAmp HS PLUS RNA amplification kit (Applied Biosystems, Cat# KIT0525) following the instructions.

RNA Sequencing and Data Analysis

1 μg amplified RNA for each sample was used for cDNA synthesis. cDNA libraries were constructed using NEB Next Ultra II DNA library prep kits (New England Biolabs, cat. no. E7645L) and adapters in VAHTS DNA Adapters set1/2 for Illumina (Vazyme, cat. N801-01/ N802-01). Libraries were then qualified on an Agilent 2100 Bioanalyzer using an Agilent high-sensitivity DNA kit (Agilent Technologies, cat. no. 5067-1513), and quantified using a Qubit dsDNA HS assay kit (Thermo Fisher Scientific, cat. no. Q32851) and an Illumina library quantification kit (Kapa Biosystems, cat. no. KK4824). All steps were performed following the manufacturer's instructions. The subsequent sequencing was carried out on an Illumina Hiseq-2500 sequencing system with 50 bp read length. The Single-end RNA-seq raw reads were aligned against the *D. melanogaster* genome (BDGP6) using STAR (v020201). The number of reads was assigned to protein-coding genes using featureCounts (v1.6.3). Significantly differentially expressed genes were identified with Padj values $\leq$ 0.01 and fold change $\geq$ 2 by DESeq2.

DamID Sequencing and Data Analysis

The DamID experiments were carried out using a previously reported modified method (Gutierrez-Triana et al., 2016). Briefly, *esg^{ts} > GFP, UAS-oDam* flies, *esg^{ts} > GFP, UAS-ttk-oDam* flies, *esg^{ts} > GFP, UAS-seq-oDam* flies, *esg^{ts} > GFP, UAS-LT3-NDam* flies, *esg^{ts} > GFP, UAS-LT3-NDam-Su(H)* flies, *esg^{ts} > GFP, UAS-ttk-IR; UAS-LT3-NDam-Su(H)* flies and *esg^{ts} > GFP, UAS-LT3-NDam-Su(H); UAS-seq* flies were used to harvest midguts after induction in 29°C for 48h. About 50 midguts were collected for gDNA isolation. The gDNA was treated with DpnII and subsequent alkaline phosphatase before digesting with DpnI. The DpnI treated samples were ligated with adaptor for ligation-mediated PCR, then followed by purification and T7 exonuclease treatment. At last, the purified samples were fragmented for high-throughput sequencing. Sequenced reads were mapped to the *D. melanogaster* genome (BDGP6) using bowtie2 (version 2.2.4). R package iDEAR 2.0 was used for establishing highly reliable profiles of transcription factor-binding sites. The density of reads in each region was normalized to the total number of 10 million mapped reads. BigWig files were generated for visualization using the Homer package.

QUANTIFICATION AND STATISTICAL ANALYSIS

All experiments were repeated at least three times unless otherwise indicated. All statistical analyses were performed using GraphPad Prism 5. ImageJ was used to count the cell numbers. For comparisons of cell numbers and gene expressions, unpaired two-tailed t tests were used to assess statistical significance. *P value*, standard error of the mean (s.e.m.) and *n* are as indicated in each figure and legend.

DATA AND CODE AVAILABILITY

All raw and processed RNA-seq and DamID-seq datasets reported in this study have been deposited in the Gene Expression Omnibus (GEO) under the accession number GEO: GSE130943.

Update

Cell Reports

Volume 33, Issue 9, 1 December 2020, Page

DOI: https://doi.org/10.1016/j.celrep.2020.108459

Cell Reports

CellPress
OPEN ACCESS

Correction

A Switch in Tissue Stem Cell Identity Causes Neuroendocrine Tumors in *Drosophila* Gut

Zhaohui Li, Xingting Guo, Huanwei Huang, Chenhui Wang, Fu Yang, Yongchao Zhang, Jiawen Wang, Lu Han, Zhen Jin, Tao Cai, and Rongwen Xi*
*Correspondence: xirongwen@nibs.ac.cn
https://doi.org/10.1016/j.celrep.2020.108459

(Cell Reports *30*, 1724–1734.e1–e4; February 11, 2020)

In the Discussion, the authors inadvertently stated that Dpn is only expressed in type II but not type I NBs. This statement is incorrect, as Dpn is expressed in both types of NBs. It is now corrected online.

The authors regret this error.